Programs for Laser-AO Assisted Integral-Field Spectrometers on Ionized Flows

Gerald Cecil

Dept. Physics & Astronomy, U. North Carolina, Chapel Hill, NC 27599

Abstract

An AO-assisted integral-field spectrograph is becoming the most efficient tool with which to explore ionized gas outflows by mapping faint spectral lines that diagnose cloud dust content, gas pressure, excitation mechanism, and chemical abundances. Coupled with recent improvements in photoionization models, the total mass hence flow energetics can be estimated. Establishing a consistent dynamical framework requires linking multi-frequency datasets to track the energy flow through its optimal-contrast emission in the various ISM phases. I show recent HST results on AGN, starburst nuclei, and Galactic Herbig-Haro Objects that cry out for complementary 3D spectra at comparable spatial resolution, to be provided soon by the laser-guided AO + integral-field spectrographs underway for the William-Herschel and SOAR telescopes.

Key words: 97.21.+a, 98.58.Ay, 98.62.Nx, 95.55.Qf

1 Introduction

In this paper, I outline some outstanding questions in the study of resolved ionized gas flows that are being addressed by combining ground-based, visible light, 3D spectra with high-resolution, filtered images from HST and other space obervatories. Inflows are often unresolved spatially and are occasionally subtle, hence can be very ambiguous. However, outflows can be both prominent and, when nearby, extensive. Outflows constrain the time evolution of binding energy, whether released by supernovae (starburst galaxies) or by gas accretion (Herbig-Haro object [HHO] flows and AGN).

I introduce some observational aspects of flows in §2. In §3 I outline the steps from observables to flow properties, show examples of our 3D work on AGN and starburst galaxy outflows to demonstrate the HST/3D synergy in action, and discuss how the main uncertainties in flow physics can be addressed by laser AO-assisted integral field spectroscopy (LAOIFS). This paper with color figures is available at `http://www.thececils.org/science/3D05.pdf`.

2 Outflows Observed

2.1 Herbig-Haro Outflows

HHO's are second only to supernova remnants as laboratories for study of non-planar astrophysical shocks. Ionization is entirely local in HHO shocks. Because only the component of motion perpendicular to a shock front is thermalized initially, gas emission depends strongly on the shock geometry hence on details of the local environment. Many shocks in HHO's are fast enough to develop a photoionized precursor. As speeds increase substantially above 150 km s^{-1}, the precursor grows and can transfer radiant energy across the flow to alter the excitation and ionization of the pre-shock gas. Increased preshock ionization raises the temperature of the post-shock gas. The flow is inherently time variable, with numerous compression/rarefaction shocks emitting in the less dense ISM that spans the $\sim 1'$ field of a ground-layer compensating AO system, while internal shocks propagate to crush small, denser ISM components. A laser is necessary because these flows are associated with molecular clouds that obscure natural guidestars.

HST has resolved ground-observed "knotty" HHO "jets" into streams of bow shocks around "bullets" that are heavier than their surroundings (Reipurth et al, 1997, for example). The multi-epoch HST images shown in Fig. 1 (Bally et al, 2002; Hartigan et al, 2001; Reipurth et al, 2002, for example) map transverse velocities and even accelerations of individual gas clumps in the bow-shock and "jet" complexes. Many classical HHO's have been studied with 3D spectra, but mostly with Fabry-Perot (FP) (López et al, 2005; Cecil, 2000, and references therein) spectrographs that focus on only a couple of visible/near-IR (VnIR) emission lines and have almost never attained better than 0.5 arcsec^2 resolution.

Without radial velocities at HST's 0.01 arcsec^2 resolution over several emission lines, there are no useful constraints on the space motions of the emitting complexes in the various shocks. Numerical simulations (Raga et al, 2002, for example) highlight that space motions are critical to understanding the evolution of the flow and flow entrainment from/deflection by the embedding molecular cloud. HST sees oblique shocks along the jets (Heathcote et al, 1996) that have the hallmarks of prompt ISM entrainment (Raymond et al, 1994). Shock velocities are low enough that no "cross-ionization" occurs from the highest velocity region near the shock apex into the wings (not the case in AGN's (Ferruit et al, 1997)). 3D FP spectra have isolated the Mach disk (the jet deceleration shock) by its excitation, kinematics, and geometry. Models of the shock emission have good microphysics (no need

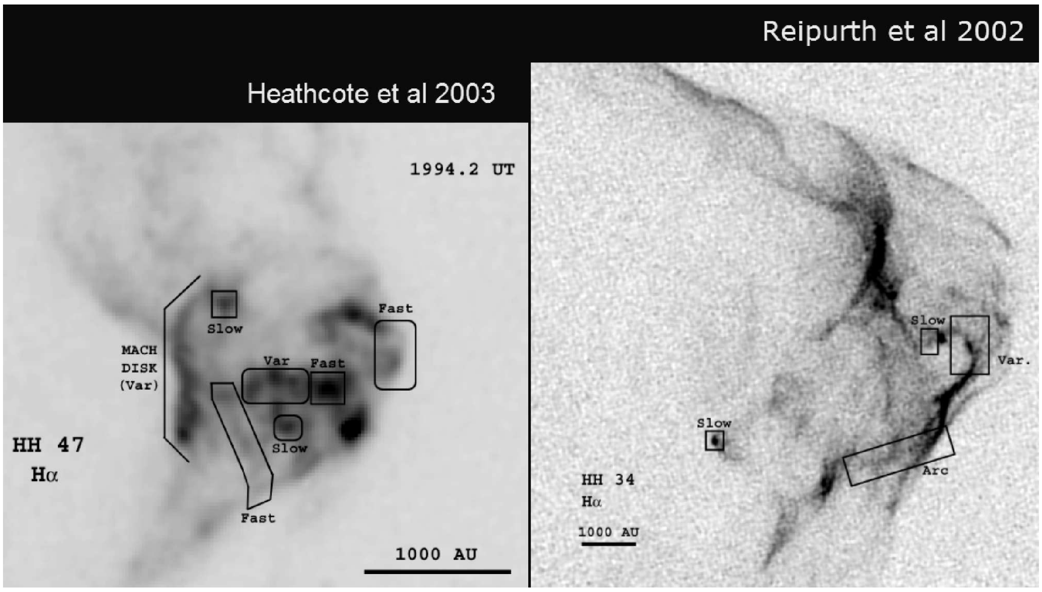

Figure 1. Snapshots from multi-epoch HST movies of two HHO bow-shocks. The region shown is 20″ on a side. Different parts flow at different transverse speeds. View the movies at `http://sparky.rice.edu/~hartigan/movies.html`.

to include the source star), schematic (3/2D model) geometry, and poor/nonexistent treatment of gas hydrodynamics. These models constrain the ionization fraction hence flow mass and the ambient B-field (which alters line ratios by limiting post-shock compression, but insufficiently to alter hydrodynamics.) Comparison with models shows a mismatch between the inferred shock speed and the observed kinematics, indicating flow into an already moving medium. Fainter bow shocks at much larger radii (Reipurth & Bally, 2001) support this view. The interpretation is that Fu-Orionis-type ejections have occurred every few hundred years over a long timespan.

2.2 AGN Outflows

Circa 1970, ground-based spectral maps began to study spatially extended regions of broad emission-line profiles in AGN, but seldom uncovered symmetries. Such "narrow-line regions" (NLR's) span $\geq$500 km s^{-1} and up to $\sim$ 12 arcsec^2 but more typically $\leq$1 arcsec^2. In AGN with a dense ISM, such velocities imply some shock emission. However, it would be surprising if shocks dominate over gravitational release because their much lower radiant efficiency requires orders of magnitude more accretion to power the observed emission.

Subsequent radio surveys (Ulvestad & Wilson, 1984, for example) showed that up to a third of Seyfert nuclei have small radio jets/plasma bubbles. AGN outflows may be more massive than observed because any thermal wind component cannot be seen in the radio (Bicknell et al, 1998). Some Seyfert radio images show an extended interaction of the outflow with the magnetized ISM for an arcsecond or several along a preferred axis; these systems (this axis) became prime targets for HST filter imaging (spectra). They are UV bright and frequently embed in slightly larger ionization cones powered by the AGN. On the ground, 3D (first FP, then the more powerful integral-field) spectrometers supplanted slits. Complete spatial coverage allowed dissection of outflows but — seldom attaining better than 0.5 arcsec^2 resolution — interpretation was confused by the blending of myriad emitting clouds.

STIS attained 10$\times$ smaller sampling and, as expected, clarified the structure of Seyfert 2 NLR's. With negligible non-stellar continuum light, emission lines in those objects are diluted only by starlight. STIS' small sampling scale therefore increases the contrast of fainter, diagnostic lines and broad wings on more intense lines (Pogge et al, 2003, for example). Such data and photoionization models constrain the average cloud but do not address the distribution of fainter outflow emission. Radial velocities of the brighter emitting clouds in most spatially extended NLR's were mapped with STIS' slitless mode by Kraemer, Crenshaw, and colleagues. But, HST scheduling constraints prevented a large sample of AGN outflows from being studied more thoroughly and sensitively with slits.

Much of an AGN outflow proceeds outside VnIR bands: radio continuum and X-ray images are important tracers but lack the spatial resolution of HST imagery and need long exposures to attain complementary plasma diagnostics to those from UV/VnIR spectra. UV spectra alone can be powerful discriminants of physical conditions in ionized gas, high-velocity shocks being particularly well characterized by strong UV lines (Allen et al, 1998). However, few UV spectral maps were made before STIS failed, because compensating for dust extinction outside the nucleus required a sequence of long exposures stepped across the NLR. Only the UV low resolution ($\sim$ 500 km s^{-1}) gratings were used.

NLR spectra are consistent with gas being photo-excitated/ionized by the power-law spectrum of the AGN. But from the ground, lumpy emission-line profiles indicate several kinematical subsystems projected along our sightline whose gas velocities often exceed 1000 km s^{-1} relative to the galaxy ISM, and occasionally show abrupt jumps near radio knots and arcs (Whittle et al, 1988). However, at the velocities characteristic of AGN, post-shock emission of hot gas from a flow into a stationary ISM mimics an AGN-like power-law. While velocity discontinuities arise naturally from shocks, the shock role in NLR's seems to be secondary or very transient. Extinction is not a problem above 0.2 keV, the photon energies accessed by gas cooling behind a >300 km s^{-1} shock. The Chandra spectrometers combine sufficient spatial/spectral resolution with enough sensitivity to map this warm gas in nearby systems, and have shown that there is very little of it in the extended, high-velocity NLR of NGC 1068 (Kinkhabwala et al, 2002). This important result should be generalized.

3 Analysis of Spectra

3.1 General Procedures

An LAOIFS operating over VnIR wavebands can obtain spectral maps at sufficient spatial resolution to deblend the emitting complex from background emission; small pixels on the sky also minimize dilution by starlight. Ideally, separation is spatio-kinematical; however, such detailed analysis is only practical for highly symmetrical flows. Once isolated in the strongest lines, the same kinematical components may be identified in weaker lines of different ionization/excitation.

Establishing the flow energy of each component is straightforward:

- Deredden its spectra across the outflow. The Balmer decrement is used under the assumption that gas is photoionized and excited to $\sim 10^4$ K. However, IFU spectra that span $\lambda\lambda 0.4 - 1\mu$m with a deep depletion CCD can exploit the blue/IR [S II] flux ratio to minimize this T sensitivity.
- Transform the flow radial velocities into the rest frame of the galaxy or star-forming region. Because kpc-scale outflows can extend into galaxy halos at considerable inclination above the galaxy disk, deprojection sometimes alters our perspective quite markedly (e.g. §3.3.5).
- If there is a clear symmetry axis, bound space velocities by assuming that the flow is either a) along the axis, or b) perpendicular to it. Both extremes occur during the evolution of simulated jets. An organized outflow will surely show kinematical gradients along the axis. Abrupt changes in radial velocity indicate flow redirection and/or acceleration/braking. Simple kinematical models of e.g. various filled biconical flows can help to build intuition of kinematical patterns and can highlight unexpected motions.
- Estimate pre-shock density n_o and gaseous filling factor of the emitting species, because ionized mass, KE, and momentum all scale by $1/n_o$. With just visible-band data, one uses recombination fluxes derived from shock models because the [S II] lines have limited dynamical range and apply only to gas of poorly constrained filling factor. AGN circumnuclear regions beyond the NLR are frequently in the low-density limit, and indeed the NLR can be inclined to the galaxy disk, introducing a strong density gradient. HHO's can flow in a dense enough ISM to use this doublet, but their comparatively low shock speed requires a large correction of the ionization fraction (Hartigan et al, 1994), knowledge of the gaseous filling factor (which is well constrained by HST images), and are again sensitive to density variations at the boundary near dense patches of the ISM.

3.2 Some Current Issues with HHO Flows

With only local pre-shock ionization, HHO shocks are inherently simpler than those in AGN. Fortunately, jet and ISM shocks are easy to separate by their different velocities hence gaseous excitation. The main limitation today is the lack of 3D spectra across the shock complexes at comparable spatial resolution to the multi-epoch HST images. Because 3D simulations are becoming powerful enough to reproduce the instantaneous appearance of a flow (Raga et al, 2002, for example), a ground-layer compensating LAOIFS program on HHO's would provide important guidance to modeling efforts to probe flows and their environments.

HST reveals very dynamic Mach disks. In 2D simulations, the disk has toroidal edge instabilities. In 3D, this axisymmetry is broken into side-to-side oscillations as the Mach disk dumps entropy. The Mach disk plays a central rôle in thermalizing the outflow. So, a detailed movie of its motions from e.g. annual images would tell us about a combination of variations in the ISM density as processed through the expanding bow-shock, and variations in "jet" flow. A ground-layer compensating LAOIFS would span the bow shock nicely.

Entrainment flows along the "jet" boundary are well delineated in HST images (Fig. 2) by collisionally excited lines like [S II], and have even better contrast in H_2. Attaining comparable resolution with a LAOIFS would allow systematic investigation of entrainment in different environments (e.g. vertical punch out vs. grazing impact of a denser cloud as evident in HH 110, top panels of Fig. 2) to constrain the "jet" thrust, improve constraints on momentum transfer to the parent cloud, and possibly even study the effect of magnetic fields. The origins of interstellar turbulence are still poorly understood, but HHO entrainment surely plays a role.

3.3 AGN NLR Spectra

3.3.1 From Observables to Filament Properties

Once components are separated, one can constrain their gaseous excitation by scatter plotting pairs of flux ratios of diagnostic emission lines that are also close in wavelength to minimize reddening uncertainties (Veilleux & Osterbrock, 1989, for example). Grids of model ratios generated with steady-state, power-law photoionization (index α between -1 and -2 is appropriate for AGN) and shock codes span the observed spectra. Especially for UV ratios, the two model grids do not overlap much, providing a simple way to isolate the dominant excitation mechanism and certain average parameters of the ionized gas.

Photoionization models (Krolik, 1999) computed grids of flux ratios for given (gas density, power-law ionization parameter) parameter pairs, initially for a single

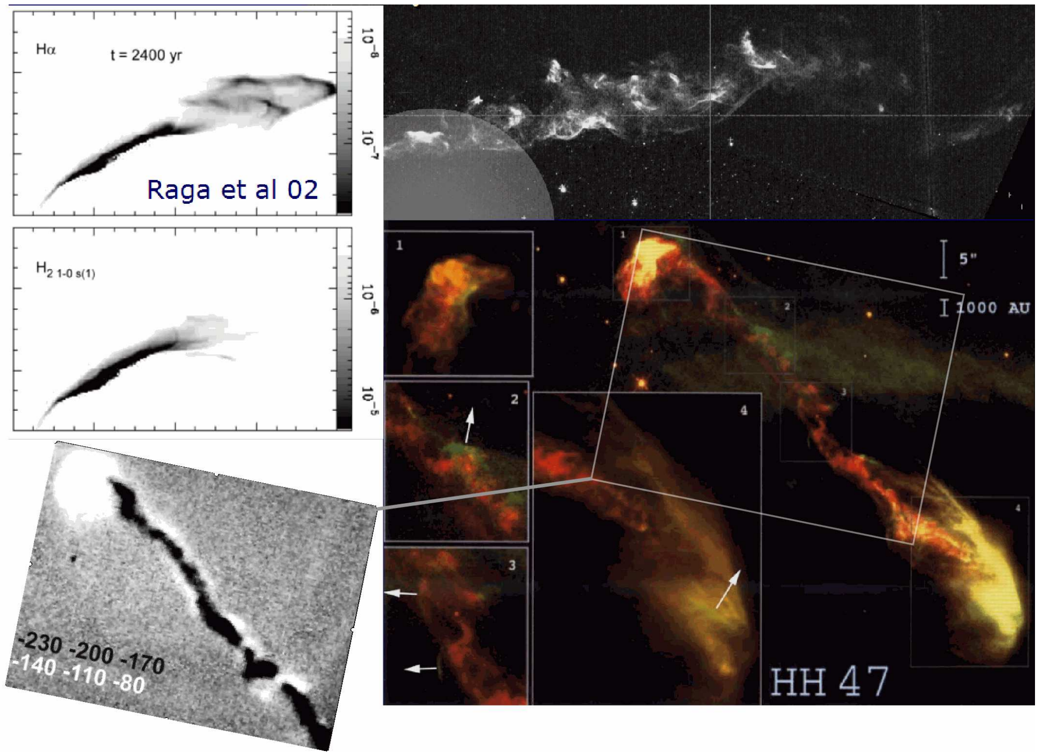

Figure 2. HHO's: observed & modeled. The panel at lower left used the Rutgers FP on the CTIO Blanco 4m to show how low and high gas velocities are segregated along the flow of HH 47. At right the HST Hα (red) and [S II] (green) color image (Heathcote et al, 1996) shows how the low velocity sheath resolves into numerous "green" shocks that penetrate the adjacent dense ISM. The HH 110 flow at upper right fragments as it is grazes a denser cloud. The simulations at upper left (Raga et al, 2002) reproduce those observations quite well, but an IFS velocity datacube would more tightly constrain the model.

cloud, occasionally for a nested set at different ionization parameters and column lengths, and finally for a combination of matter and ionization bounded clouds the so-called $A_{M/I}$ sequence (Binette, Wilson, & Storchi-Bregmann, 1996). By bounding the full extent of the cloud mass, not just its ionized sheath, these models better estimate the flow kinetic energy and mass loss.

Fig. 3 shows how our STIS spectra spanned half of the NLR of NGC 1068. Panel (b) shows a slice of [O III] profiles along the axis of the ionization cone. STIS's 0.″2-wide slit and 0.″05 resolution along the slit has deblended this large NLR into discrete clouds and has delineated their radial velocities. There are amazing knots in this half of the NLR (Cecil et al, 2002), evident as 2000 km s^{-1} wide "streaks" (e.g. insert profile in panel (b)) that are found only on the blue wings of the line profiles $\sim 1''$ (70 pc) closer to the nucleus than a region of very high-ionization coronal lines (Kraemer & Crenshaw, 2000; Marconi et al, 1996). The same clouds are present in the brightest UV lines; Fig. 4 plots their UV flux ratios and compares them both to shock models (left panels) and to various photoionization models (right panels) that we now discuss.

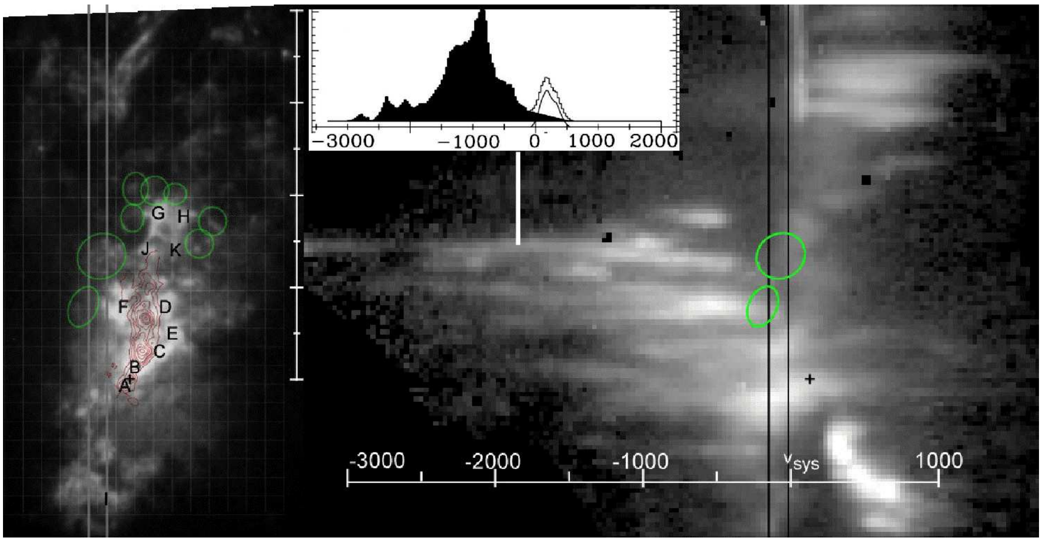

Figure 3. (a) HST/FOC [O III] image of the NLR of NGC 1068 (Cecil et al, 2002); we show the first of 5 vertical slits that covered the middle third with HST/STIS spectra. Vertical ticks are at 0.″5 intervals. The background grid shows GMOS IFS samples. (b) An example of the [O III] profiles obtained by STIS that is here extracted along the line shown at left. Velocities are relative to galaxy systemic. The insert plots the [O III] emission profile of one component.

3.3.2 Accounting for Dust in Emitting Filaments

Photoionization models can fit observed NLR line fluxes successfully, but the tuning has unsatisfactory aspects:

- Model gas temperatures are often inconsistent with values obtained from observed nebular diagnostics. This "O^{++} problem" was solved notionally with the $A_{M/I}$ sequence, an *ad hoc* sum of different emitting regions.
- To reproduce the fluxes of very highly ionized coronal lines, a region with very high ionization parameter must usually be added along the same sightline as gas at much lower ionization. The connection between regions is not addressed except to say that one component "filters" the other.
- Observed flux ratios are very similar among AGN, so are modeled successfully using only a very small range of a much larger possible span of U values.
- Large velocity gradients and discontinuous jumps are features of those AGN NLR's that have been studied in detail, yet are unexplained in a photoionized plasma.

Groves, Dopita, & Sutherland (2004) appear to have resolved these deficiencies. Motivated in part by our STIS spectral maps of the high-velocity "streaks" in NGC 1068's NLR (Figs. 3 & 4), they added dust absorption to the photoionized cloud. Fig. 5b shows how dust changes the internal pressure of the model cloud from constant density to isobaric; see Dopita et al (2002) for details. Panel (c) from Groves, Dopita, & Sutherland (2004) show how this modification greatly expands

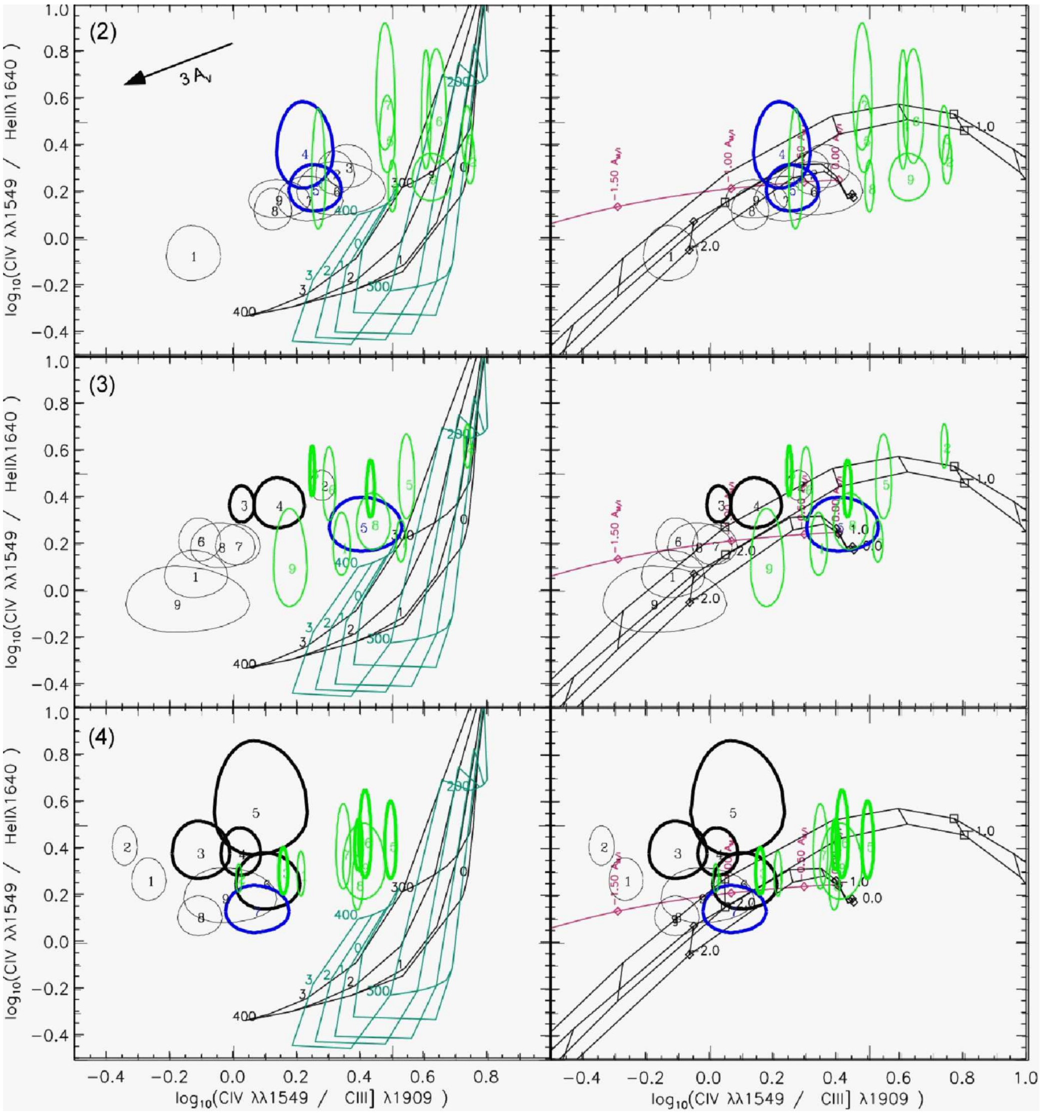

Figure 4. HST/STIS UV flux ratios along 3 cuts across the NLR of NGC 1068, compared to shock (left) and various photoionization models (right). $\pm 1\sigma$ uncertainty ellipses are shown on the observed spectral ratios, which are best fit by photoionized, isochoric clouds (Groves et al, 2004).

the range of $U's$ that reproduce the observed line ratios, no longer needing to be fine tuned over a narrow set of U for concordance. The range of U in their model mimics that of the $A_{M/I}$ sequence, but now with a plausible distribution arising from varying cloud dust load and size. Panel (d) shows how dust reduces the "O^{++} problem".

In Groves et al (2004), we compare both dusty and dustless photoionization models with our STIS UV data of NGC 1068. The left-hand column of Fig. 4 shows that shock models were clearly inconsistent, but that either photoionization model at right reproduces the observed ratios across this NLR.

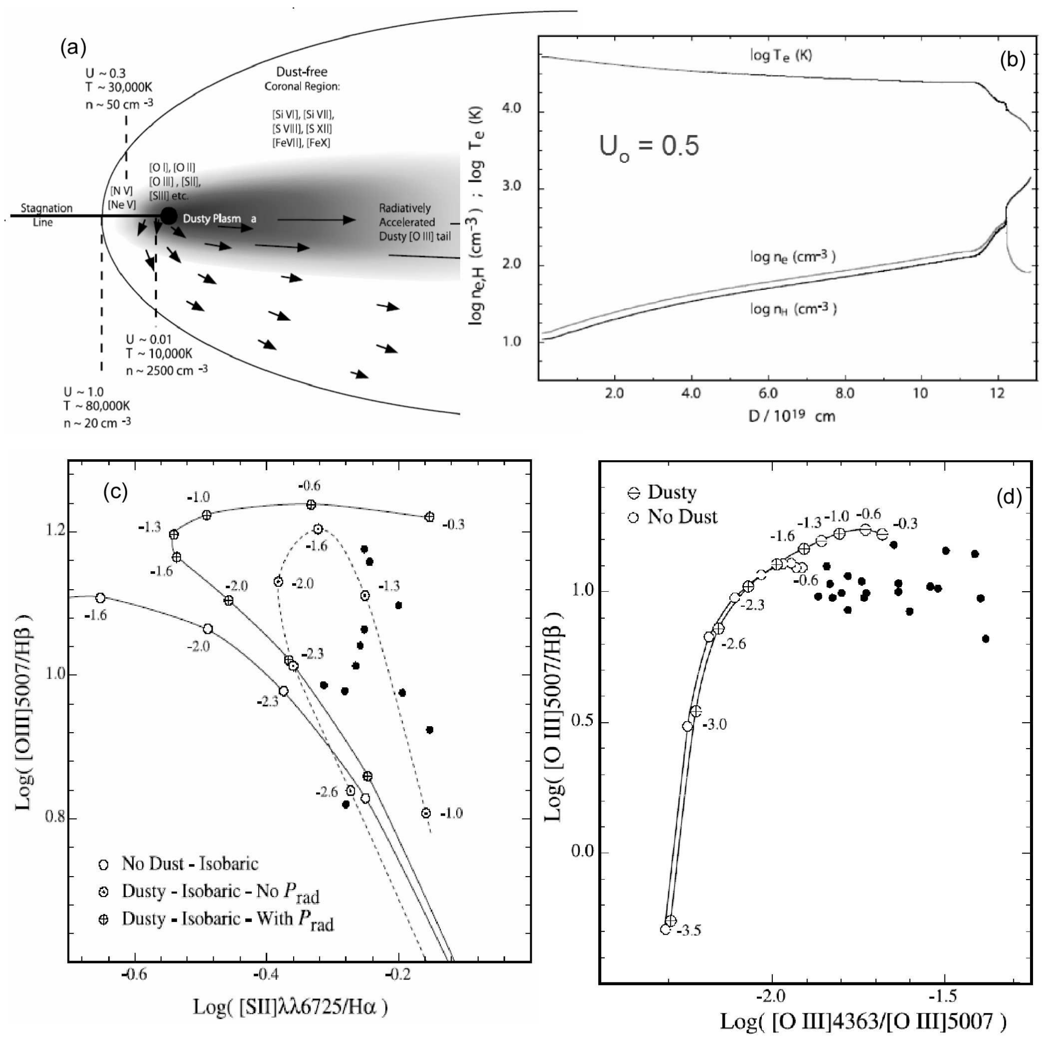

Figure 5. (a) Schematic model of a dusty gas cloud undergoing radiative acceleration. At various points in the flow, the average ionization parameter U, gas temperature, and density is shown. (b) The resulting internal structure of the emitting cloud. (c) Photoionization models with and without dust, plotted on a space defined by emission-line ratios that are robust to reddening uncertainties. Models track variations of the line ratios for different U on the cloud. The dots are from spatially integrated spectra of various AGN. (d) The X-axis is a diagnostic emission-line flux ratio that is sensitive primarily to gas temperature. Note how the dust-free cloud stagnates along the X-axis as U increases. In contrast, the dusty model continues to report higher O^{++} temperatures with higher U (Groves, Dopita, & Sutherland, 2004).

The dusty models are plausible and straightforward resolutions of long-term conundrums in AGN spectra. Groves, Dopita, & Sutherland (2004) compare spatially integrated NLR data to the models shown in Fig. 5c to improve estimates of global NLR properties. NLR dynamics can now be explored reliably with spatially resolved spectra of individual NLR's. One should start with NGC 1068, using the STIS spectra as a guide. This NLR should be mapped with an LAOIFS to minimize blending. A 4m telescope is adequate for a few NLR's, but the important diagnostic lines are faint and pixels are small, requiring a photon counting CCD and/or an 8+m telescope. Many Seyfert 2 nuclei are unsuitable for locking an NGS system, requiring a laser.

3.3.3 Insights from Simulated Cloud/Outflow Interactions

Real flows are not characterized by a single, steady shock velocity! Numerous shocked filaments intersect, each with post-shock temperature $T_s \simeq 1.1 \times 10^5 v_s/(100$ km s$^{-1}) > 2 \times 10^5$ K for fully ionized gas. In hypersonic flows through all but the most rarefied ISM, gas cools as shocks crush pre-shock density fluctuations. Cooling introduces global shock oscillations as gas collapses, clearly evident in simulations as large-scale pulsations. In HHO and AGN shocks, gas densities are high enough for prompt radiative cooling. For AGN shocks, $L_{cool} = 11.3 V_{s300}^4 / n_o$ pc (units of 300 km s^{-1} and cm^{-3}.) Less KE becomes pressure compared to a steady-state shock. So, steady-flow models underestimate shock velocity and overestimate preshock gas density.

Whenever the flow overruns a denser ISM cloud, a bow shock first detaches cloud from flow and the shocked flow then compresses/crushes the cloud by propagating a slow reflection shock. The reflection shock is generally not observed with visible-band spectra but can be prominent in the near-IR. Failing to account for dense clouds alters our interpretation of the flow in two ways. First, clouds crushed by shocks evolve rapidly through localized cooling that saps the outflow's over-pressure. Second, clouds ablate, thereby enhancing flow emissivity and returning dusty material to the gas phase.

Clouds therefore soon develop a core/structured halo. Filaments in the halo disappear by photo- or thermal-evaporation before moving far from the core, dumping dust along the way. Hydro-thermal instabilities evaporate clouds after
$t_{evap} = (n_c/1000\,cm^{-3})(r_c/pc)^2(T_f/10^7 K)^{5/2}(\ln C/30)$ Myrs, with n_c the embedded cloud density, r_c its radius, T_f the temperature of the bulk flow, and C the Coulomb logarithm. This would imply that only large, dense clouds can survive longer than 1 Myr. However, (Ferrara & Shchekinov, 1993) found that clouds cease evaporation once crushed to optical thickness $\tau > 1$. Clouds may therefore survive to reach much of the flow speed if they do not exit the flow. Schiano, Christiansen, & Knerr (1995) show that the halo penetrates only to the depth of the Kelvin-Helmholtz (KH) instabilities. The halo ablates from the unscathed core, dumping the entropy induced by the enveloping shocked flow in a series of "shedding events" that "fire polish" the cloud surface to reset the KH clock. By ablating small bumps, the cloud core apparently stabilizes itself against disruptive larger instabilities and can survive to accelerate toward the flow speed.

3.3.4 AGN Bow Shocks Observed

To date, fewer than 20 AGN NLR's have been studied with 3D VnIR spectra. Most were selected because they contain radio jets. We need an unbiased 3D survey that does not depend on source features. With an LAOIFS, a 4m telescope can work on nuclei without a compact light source on which to lock the AO system. There are surprisingly few targets otherwise.

Spirals are preferred environments because their dense ISM prolongs the interaction even for outflows that punch out of the galaxy disk (e.g. TIGER IFU data on the N bow-shock in NGC 1068 (Pécontal et al, 1997).) Some AGN bow-shocks do appear to be moving into a more rarefied medium; the outflow of NGC 1068 is inclined 45°above the galaxy disk, while that of NGC 4258 is inclined 30° (§3.3.5).

AGN 3D spectra have to date often been limited to a few lines on a messy background. An IFS on a larger telescope allows effective spatial binning to build up the S/N for faint lines such as the temperature diagnostics [O III]λ4363 and [N II]λ5755. At present there are limited constraints on chemical abundances and only a few near-IR species such as Fe and H_2 that address possible cloud shocks; powerful IFS such as SINFONI are changing this. Post-shock gas is prominent in X-rays, but its chemical abundances have not been measured reliably to date because of uncertainties in the filling factor of warm gas (Strickland et al, 2004).

3.3.5 NGC 4258: Multifrequency Jet/ISM Interaction

An interesting jet/ISM interaction is the nearby (7.2 Mpc) spiral galaxy NGC 4258 (M 106), with the added benefit that the spatio-kinematic distribution of masers imply a compact circumnuclear disk (Miyoshi et al, 1995). Our work has focused on understanding the nature of the large-scale ($5'$) "anomalous arms" (Fig. 6), which have been characterized as twisted jets that are rising bouyantly out of the galaxy disk (Daigle & Roy, 2001, for example) to feed the large-scale radio lobes. Jets and accretion disks are certainly linked in the minds of theorists, but observational connections are tenuous. NGC 4258 is unique because the active flow can be traced continuously for an arcminute down to the VLBA-scale flow above the maser disk (Cecil et al, 2000, for example).

The anomalous arms emit most of the radio synchrotron and X-rays of the galaxy. They are also evident in line species e.g. [N II]λ6583 favored by shock excitation or X-ray heating (Cecil, Morse, & Veilleux, 1995). The large spatial extent of the thermal (Wilson, Yang, & Cecil, 2001) X-rays along the anomalous arms also indicate fast shocks consistent with the observed kinematics of the ionized gas. Our multi-configuration VLA image (Fig. 6 from Cecil (2000)) isolated the active jet within the anomalous arms. The jet projects NS close to the spin axis of the accretion disk. The active flow ends in oblique shocks. We show in Wilson, Yang, & Cecil (2001) that the jet particles extend 30° above the galaxy disk, and that their

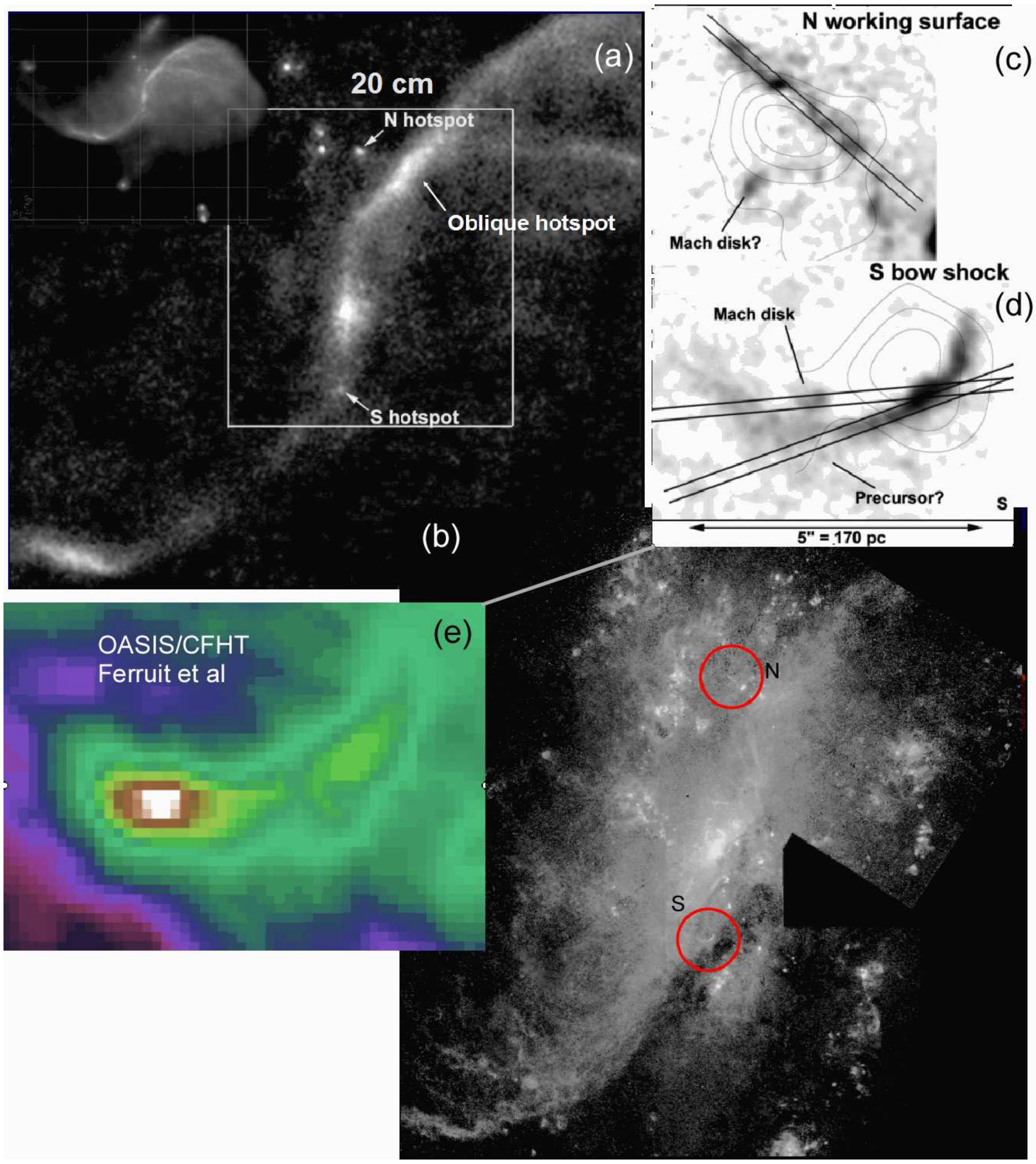

Figure 6. (a) λ20 cm VLA image of NGC 4258. The main image spans $3 \times 3'$. The insert shows 3× the area, and the full outflow across much of the galaxy at lower resolution and with more sensitivity to diffuse emission. The active jet flows almost NS to end at prominent hotspots. (b) The HST image of combined [N II]+Hα shows ionized gas associated with the radio arms. N and S shock complexes around the jet termini are circled. (c) & (d) Closeups of the N & S shock complexes in ionized gas, together with proposed STIS slit locations to sample structures along the flow. The contours show the radio hotspots evident in (a). (a)-(d) are from (Cecil et al, 2000). (e) The S bow shock as seen by the OASIS IFS on CFHT (Ferruit et al in prep), at the same scale as panels (c) & (d).

ionizing radiation field is being absorbed by the nearest dense gas in the galaxy below to produce most of the thermal X-ray emission (Fig. 8).

Pairs of long-slit B to R spectra that we obtained at the WHT (Fig. 7) span both the N and S shock complexes ("poor man's 3D"). We then modeled the observed

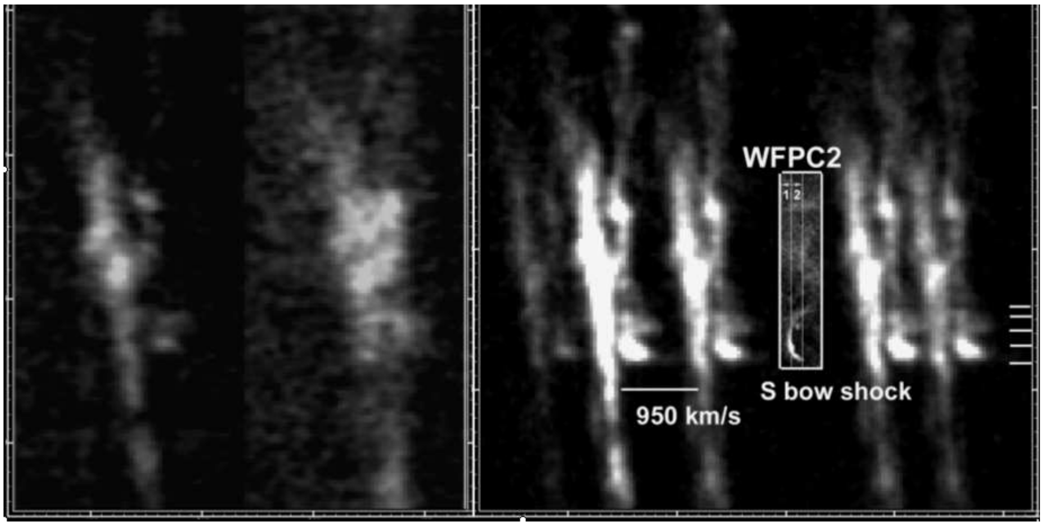

Figure 7. The S bow shock in NGC 4258, obtained with the WHT/ISIS 2-beam spectrometer placed along the shock front. [O II], [O III], Hα, [N II] and [S II] emission-line profiles are shown left to right, together with HST/WFPC2 discovery image at the same spatial scale. The apex of the shock is near the systemic velocity of the galaxy, with the wings increasingly redshifted (Cecil et al, 2000).

patterns as a "3/2D" paraboloidal bow-shock to pin down its geometry and to interpret velocities in the frame of the rotating galaxy. We find that the apex of the S bow shock has almost stalled and emits near the velocity of the bar-forced galaxy disk. Elsewhere, radial velocities hence space velocities of gas in the shock increase away from the apex as the wings advance. The shock velocity from our models is consistent with that expected from our measured line ratios. The Balmer decrement yields $A_V = 1$ for both shocks, permitting detailed optical spectra (but preventing reasonable exposures for STIS UV spectra). Nearby, "fossil" versions of these features lag galaxy rotation at similar radii.

The very clear S bow shock is scaled perfectly for IFS studies at high spatial resolution! A "proof of concept" with OASIS at CFHT is shown in Fig. 6e (Ferruit et al in prep.), but deeper exposures in better weather are required. There are bright knots both interior to and at the bow with radial velocities suggestive of a Mach disk or cloud shock. Spectra at higher angular resolution could establish their dynamical role. Note that 3/2D bow-shock models do not address Mach disk emission.

There are a handful of other LAOIFS-scale bow shocks known in nearby galaxies. NGC 2110 has been studied by Ferruit et al (2004) with HST filter images and by Pogge et al (private communication) with a single HST/STIS spectrum, Whittle & Wilson (2004) have studied those in Mkn 78 with HST, and the bow shock of NGC 1068 was studied with TIGER at CFHT by Pécontal et al (1997).

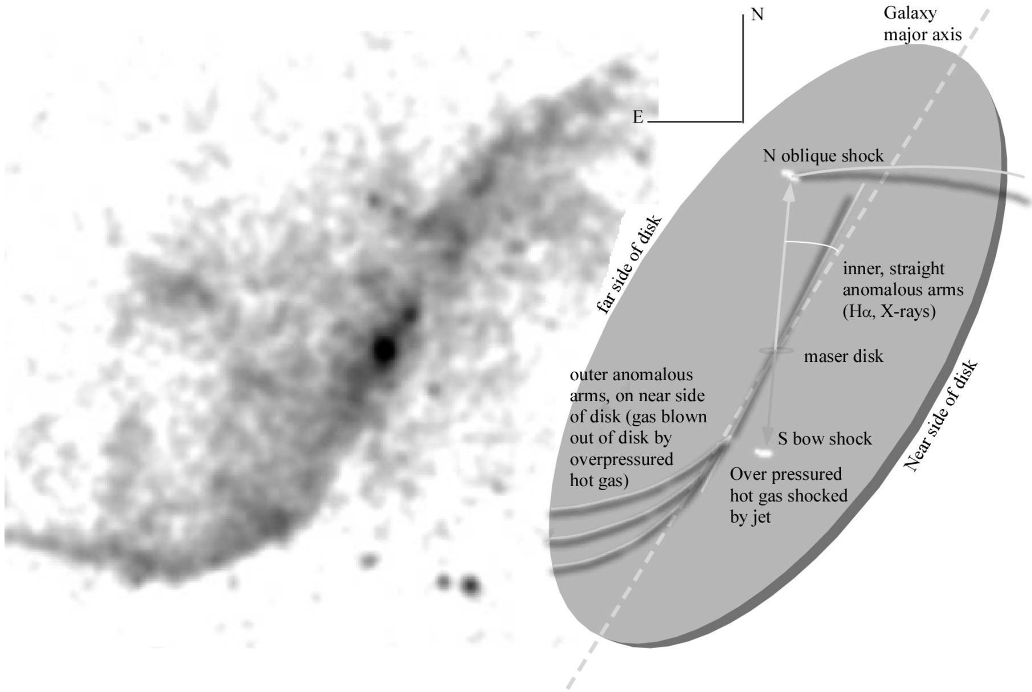

Figure 8. (Left) Chandra image of the jet and anomalous arms of NGC 4258, smoothed to 2.″7 FWHM, which covers the same area as panels (a) & (b) of Fig. 6. (Right) interpretative cartoon of the X-ray and optical line emission across its NS jet and the inner anomalous arms (Wilson, Yang, & Cecil, 2001). The orientation of bow shocks, inclination of the maser disk, projection angle of the active radio jet, and the "line of damage" from X-ray emission on the galaxy disk all argue that the jets have not precessed over the lifetime of the inner, 6 kpc-long flow.

3.3.6 Ring Shock & Fueling Feedback of a Steady-State Galactic Wind Flow

More energetic outflows into a denser ISM — such as those associated with the over-pressured galaxy-scale wind from a starburst nucleus — can inflate a superbubble that rises high above the galaxy disk. Superbubbles may prevail in the high redshift universe, so local studies of well resolved prototypes are important. We summarize the relevant flow scalings and physics in our recent review of galaxy winds (Veilleux, Cecil, & Bland-Hawthorn, 2005). Mass loading of the wind can cause RT instabilities to culminate in repeated, large vortices that crush gas along shocks as the bubble apex shreds; such features are evident in the new 3D simulations shown in the lower panels of Fig. 9. Elsewhere the flow can be almost adiabatic, progressing so rapidly that the timescales for recombination, collisional ionization, and excitation exceed greatly the dynamical time (Breitschwerdt & Schmutzler, 1999). The gas soon becomes very convoluted, with a fractal size distribution that Sutherland, Bicknell, & Dopita (2003) show enhances cooling, hence shock prominence, compared to steady-flow models.

Outflow fueling is an important subject with few observational constraints. In AGN studies, proposed schemes are fragile (Emsellen, 2004, for example). In contrast,

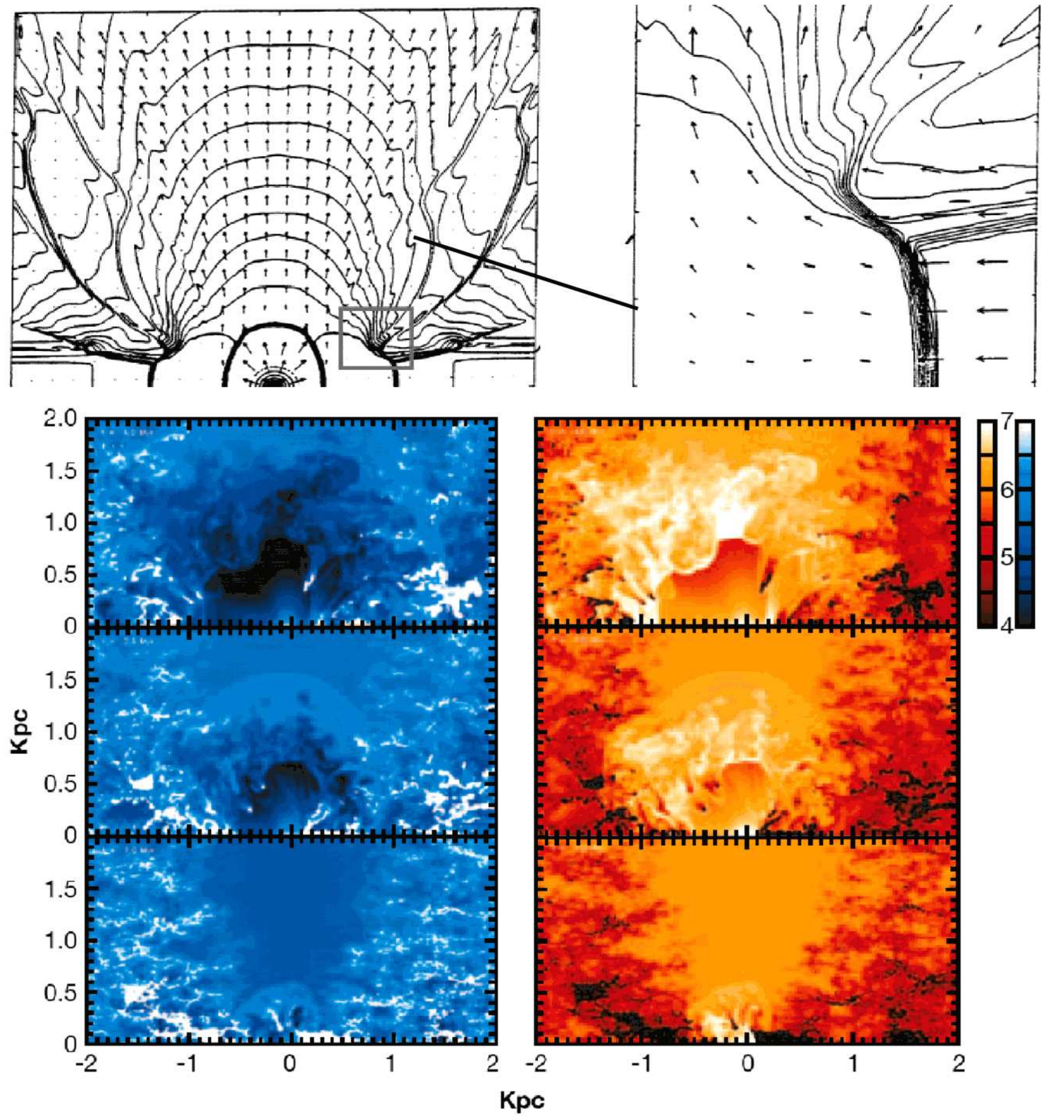

Figure 9. (Top row) A 2D axisymmetric model of galactic wind outflow by (Tenorio-Tagle & Muñoz-Tuñón, 1997, 1998) that shows pressure contours and velocity vectors of the flow in its steady-state configuration. The panel at left shows the whole flow, the closeup at right details of the "ring" accretion shock in the disk plane of the galaxy. (Bottom) 3D gas simulations of an expanding galaxy-scale wind bubble by Cooper, Bicknell, & Sutherland (private communication) showing the cooling rate at left and T at right.

steady, wind-driven large-scale flows can develop a "stagnation ring accretion shock" in the disk plane, see Fig. 9. Tenorio-Tagle & Muñoz-Tuñón (1997, 1998) show how this shock becomes prominent when the ram pressure of even diffuse H I augments the thermal pressure of the enveloping gas. Fueling stalls the ring at almost constant radius, a result consistent with the sparse kinematical data on ring shocks. However, a LAOIFS can make significant progress because ring shocks will be edge brightened and, in edge-on systems observed at high spatial resolution (e.g. NGC 3079 described in §3.3.7), the shock is less confused by unrelated background emission. Characterizing this shock also addresses the more general issue of feedback be-

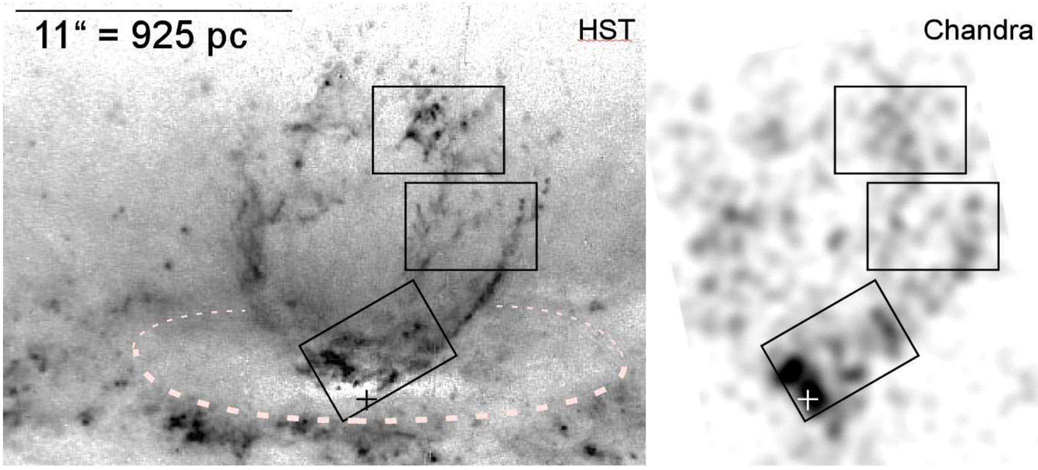

Figure 10. Highlights of the nuclear superbubble of NGC 3079 in (left) [N II]+Hα, with Chandra (right) (Cecil, Bland-Hawthron, & Veilleux, 2002). The accretion ring shock lies along the dashed line. Patterns probably from Rayleigh-Taylor instabilities are evident at the apparent vortex at the top of the bubble. Gas is concentrated into four vertical towers in the walls. These are often unresolved at HST dithered WFC resolution, tightening the constraint on the gaseous filling factor that we derived from our ground-based FP spectra (Veilleux et al, 1994).

cause the shock controls the minimum mass that must be accreted to sustain the starburst hence outflow.

3.3.7 Galaxy Wind Bubbles Observed

NGC 3079 is an almost edge-on spiral with energetic star formation in its disk. The whole galaxy disk is ejecting narrow gas and dust filaments. It has a prominent 1 kpc-diameter, ovoidal superbubble with apex on the nucleus (top row of Fig. 10.) The bubble walls are composed of towers of gas dense enough to depolarize the emission from embedded relativistic particles. Several rings of radio emission at larger nuclear distance but of similar size suggest an episodic outflow.

Our FP datacube (Veilleux et al, 1994) sorted out the geometry and, combined with our HST data, allowed Cecil et al (2001) to tighten constraints on the filling factor, hence KE and momenta, 50-fold over our FP spectra. HST shows that the emitting towers are remarkably similar in shape, suggesting that the top half of the flow has ruptured into a large-scale vortex. Our FP datacube mapped only Hα and [N II]$\lambda\lambda 6548, 6583$ line profiles. These maps allowed us to isolate Hα fluxes, constraining the ionized mass of each filament complex. Fig. 10 shows that the bubble filaments also emit X-rays. The correlation is very tight, indicating warm sheaths around the Hα emitting material that arises from conductive heating from a bubble filled with very hot (10^{10} K), shocked wind, or from localized bow-shocks around each filament where a free-flowing wind encounters an obstruction.

Similar high-resolution Hα/X-ray studies have been made of the M82 outflow (Westmouquette, Gallagher, & Smith, 2005), the NGC 1569 outflow (Martin, Kobulnicky, & Heckman, 2002), and in the survey of Strickland et al (2004). Clearly, we must characterize the properties of the ionized filaments more thoroughly to better constrain the origin of the X-ray emission. The nearest systems are big so will require several IFS pointings (e.g. Fig. 10), but the opportunities to explore multi-kpc scale outflows are worth the effort. The several hundred parsec-scale outflow from our Galaxy provides additional incentive.

4 Summary

Despite obvious source points, AGN and HHO flows need the serendipity lacking with slits. Reconnaissance with FP's has found kinematic discontinuities characteristic of shocks. Together with HST's powerful cameras in the visible and ground-based AO for the near-IR, a 4m telescope with an LAOIFS such as those under way for the William-Herschel and SOAR telescopes can learn much on gas dynamics, and particularly on the host/AGN and molecular cloud/HHO connections.

Acknowledgements

My contribution to the work described here has been supported by NASA and NSF. I thank the SOC for travel support to this very informative workshop.

References

Allen, M. et al 1998, ApJ, 493, 571
Bally, J. et al 2002, AJ, 123, 2627
Bicknell, G. V., et al 1998, ApJ, 495, 680
Binette, L., Wilson, A.S., & Storchi-Bergmann, T. 1996, A&A, 312, 365
Breitschwerdt, D. & Schmutzler, T. 1999, A&A, 347, 650
Cecil, G. 2000, in *Imaging the Universe in 3D*, ASP Conference Series, Vol 195, W. van Breugel & J. Bland-Hawthorn (eds.), p. 263
Cecil, G., Bland-Hawthorn, J., Veilleux, S., & Filippenko, A.V. 2001, ApJ, 555, 338
Cecil, G., Bland-Hawthorn, J., & Veilleux, S. 2002, ApJ, 576, 745
Cecil, G. et al 2002, ApJ, 568, 627
Cecil, G. et al 2000, ApJ, 536, 675
Cecil, G., Morse, J.A., & Veilleux, S. 1995, ApJ, 452, 613
Daigle, A. & Roy, J-R. 2001, ApJ, 552, 144

Dopita, M.A., Groves, B.A., Sutherland, R.S., Binette, L., & Cecil, G. 2002, ApJ, 572, 753
Emsellem, E. 2004, in *Coevolution of Black Holes & Galaxies*, Carnegie Observatories Astrophysics Series, Vol 1, ed. L. Ho, in press
Ferrara, A. & Shchekinov, Yu 1993, ApJ, 539, L9
Ferruit, P., Binette, L., Sutherland, R.S., & Pécontal, E. 1997, A&A, 322, 73
Ferruit, P. et al 2004, MNRAS, 352, 1180
Groves, B.A., Cecil, G., Ferruit, P., & Dopita, M.A. 2004, ApJ, 611, 786
Groves, B.A., Dopita, M.A., & Sutherland, R.S. 2004, ApJS, 153, 9
Hartigan, P. et al 2001, ApJ, 559, L157
Hartigan, P., Morse, J.A., & Raymond, J.C. 1994, ApJ, 436, 125
Heathcote, S. et al 1996, AJ, 112, 1141
Kinkhabwala, A. et al 2002, ApJ, 575, 732
Kraemer, S. & Crenshaw, M. 2000, ApJ, 544, 763
Krolik, J. 1999, *Active Galactic Nuclei*, Princeton University Press: New York, Chapter 10
López, R. et al 2005, Astron. Astroph., 432, 567
Marconi, A. et al 1996, A&A, 315, 335
Martin, C.L., Kobulnicky, H.A., & Heckman, T.M. 2002, ApJ, 574, 663
Miyoshi, M. et al 1995, Nature, 373, 127
Pécontal, E. et al 1997, Ap&SS, 248, 167
Pogge, R.W. et al 2003, in Active Galactic Nuclei, ASP Conf. Series, Vol 290, (eds. S. Collin, F. Combes, & I. Shlosman), p. 239
Raga, A. et al 2002, A&A, 392, 267
Raymond, J.C. et al 1994, ApJ, 434, 232
Reipurth, B., & Bally, J. 2001, ARAA, 39, 403
Reipurth, B. et al 1997, AJ, 114, 757
Reipurth, B. et al 2002, AJ, 123, 362
Schiano, A.V.R., Christiansen, W.A., & Knerr, J.M. 1995, ApJ, 439, 237
Strickland, D.S. et al 2004, ApJ, 606, 829
Sutherland, R.S., Bicknell, G., & Dopita, M.A. 2003, ApJ, 591, 238
Tenorio-Tagle, G. & Muñoz-Tuñón, C. 1997, ApJ, 478, 134
Tenorio-Tagle, G. & Muñoz-Tuñón, C. 1998, MNRAS, 293, 299
Ulvestad, J. & Wilson, A.S. 1984, ApJ, 278, 544
Veilleux, S. et al 1994, ApJ, 433, 48
Veilleux, S., Cecil, G., & Bland-Hawthorn, J. 2005, ARAA, in press
Veilleux, S. & Osterbrock, D. 1989, ApJS, 63, 295
Westmoquette, M.S., Gallagher, J.S., & Smith, L.J. 2005, in *Starbursts: From 30 Doradus to Lyman Break Galaxies*, (eds. R. de Grijs and R.M. Gonzalez Delgado), Astrophysics & Space Science Library Vol. 329. Dordrecht: Springer, p. 85
Whittle, M. et al 1988, ApJ, 326, 125
Whittle, M. & Wilson, A.S. 2004, AJ, 127, 606
Wilson, A.S. & Raymond, J.C. 1999, ApJ, 513, 115
Wilson, A.S., Yang, Y., & Cecil, G. 2001, ApJ, 560, 689